Single-molecule field-effect transistors: carbon nanotube devices for temporally encoded biosensing

D. Lynall[1] and K. L. Shepard[1]
[1]Department of Electrical Engineering, Columbia University, New York, NY, USA
email: dgl2129@columbia.edu, shepard@ee.columbia.edu

2022 IEEE International Electron Devices Meeting (IEDM) | 978-1-6654-8959-1/22/$31.00 ©2022 IEEE | DOI: 10.1109/IEDM45625.2022.10019504

***Abstract*—**Observation of biomolecular interactions at the single-molecule level reveals kinetic information crucial for understanding biophysical processes and provide the basis for a new class of molecular diagnostics based on time-domain analysis of molecular interactions. Point-functionalized carbon nanotubes, otherwise known as single-molecule field-effect transistors (smFETs), have shown significant advantage over fluorescence-based approaches for such single-molecule applications due to their high measurement bandwidths, virtually unlimited observation times, low cost, and capabilities for integration with CMOS in large arrays. Here, we demonstrate the capabilities of single-molecule field-effect transistors to measure DNA hybridization kinetics and to selectively detect small molecules through conformational changes of a single-stranded DNA aptamer. In both cases, kinetics can also be modified electrostatically by changes in the bias between the smFET and the surrounding electrolyte.

I. Introduction

Single-molecule measurement techniques enable the real-time study of the kinetics of molecular interactions and conformation changes. Time-domain measurements on individual molecules reveal intermediate reaction pathways, conformational state changes, and other biophysical phenomena that would be otherwise hidden in ensemble measurements.

Point-functionalized single-walled carbon nanotubes (CNTs) have emerged as a promising platform for high-bandwidth, label-free detection of single-molecule state and single-molecule interactions[1]. This platform relies on the tethering of an individual probe molecule to the surface of a CNT. Upon binding to a specific target molecule, direct charge transfer or a change in the conformational state of the probe causes a local perturbation in the CNT surface potential which is strongly coupled to the overall conductivity of the CNT due to the one-dimensional confinement of charge carriers. When configured as the conductive channel in a field-effect transistor, the CNT plays the role of a transducer, converting conformation changes in the probe molecule or probe-target interactions into fluctuations in current resembling random telegraph noise (RTN). This device configuration is referred to as the single-molecule field-effect transistor (smFET).

Here, we present methods for realizing smFET devices and demonstrate their capabilities in observing and electrostatically manipulating molecular kinetics and in detecting biomolecules through specific probe-target interactions.

II. Fabrication of smFET Devices

A. CNT FET fabrication and characteristics

To achieve high-yield, wafer-scale assembly of smFET devices, growth of CNTs at pre-defined locations is crucial. CNT nucleation sites are pre-patterned on thermally oxidized (285 nm SiO_2) p^{++} Si substrates by electron beam lithography. The nucleation sites consist of a ~3-4 nm thick layer of Co with lateral dimensions of 3 × 3 µm deposited by electron beam evaporation in an ultra-high vacuum chamber. **Fig. 1(a)** and **(b)** show AFM scans of a Co CNT nucleation site. CNTs are grown by chemical vapor deposition (CVD) with conditions optimized such that each catalyst point yields only one or a few CNTs. Further information about the CNT growth is reported elsewhere[2]. SEM images of as-grown CNTs are shown in **Fig. 1(c), (d),** and **(e)**. Ti (60 nm) source and drain electrodes are defined by electron beam lithography and deposited by electron beam evaporation. **Fig. 2(a)** shows an SEM image of an electrically contacted CNT. After Ti deposition, the source and drain electrodes are masked and a layer of Ti (5nm) / Pt (35 nm) is deposited for the on-chip liquid gate electrode (**Fig. 2(b)**). Finally, the chip is wire bonded to a land grid array (LGA) package and a PDMS microfluidic channel is stamped over the device to allow for liquid experiments on a custom PCB containing 58 independent readouts that are simultaneously interrogated in real time. A schematic representation of a CNT FET is shown in **Fig. 2(c)** and a typical transfer curve exhibiting p-type, depletion mode behavior is shown in **Fig. 2(d)**.

B. Electrically controlled CNT point-functionalization

Point-functionalization of the CNT side-wall is achieved through the formation of a stable defect of sp^3 hybridized carbon atoms in the sp^2-bonded lattice[3]. The sp^3 defect is formed by a liquid-gate-voltage- (V_{LG}-) driven diazonium reaction on the electrically contacted CNT devices. The single covalent defect site serves as a scattering point within the CNT that is sensitive to local electrostatic perturbations. For the diazonium reagent, we use 4-formylbenzene diazonium hexafluorophosphate (FBDP) which provides an aldehyde end-group that can be covalently linked to an amine group through an imine reaction[4]. Since the initial diazonium reaction requires free electrons at the CNT surface, the sp^3 defect formation can be controlled electrically through the liquid gate. At negative biases ($V_{LG} \approx$ -0.5 V), the CNT is depleted of electrons and the reaction is essentially disabled. Positively increasing the bias increases the free electron density in the CNT, enabling the reaction to occur. **Fig. 3** shows time traces of the current

through a CNT exposed to FBDP solution at V_{LG} = -0.5 V (**Fig. 3(a)**) and V_{LG} = 0 V (**Fig. 3(b)**). The sp^3 defect formation is observed in real-time through the discrete steps in the CNT conductance when V_{LG} is held at 0 V. A single sp^3 defect is formed on the CNT side-wall by disabling the reaction electrically through increasing V_{LG} shortly after one conductance step occurs.

C. Observing DNA hybridization kinetics

The smFET platform was initially applied to study DNA conjugation and melting dynamics[5]. A single stranded probe DNA sequence was covalently attached to a CNTFET and the two-level fluctuations in the conductance were measured in the presence of the complimentary DNA target. Characteristic time traces of the smFET conductance and their histograms are shown in **Fig. 4**. The DNA melting curves shown in **Fig. 5** were extracted from the temperature dependence of the two-level fluctuations for two different oligonucleotide probe sequences. DNA hybridization kinetics were studied by extracting the dwell times of the high (τ_{high}) and low (τ_{low}) conductance states by idealizing the transitions using a hidden Markov model. Representative time trace data and the idealized fit are depicted in **Fig. 6(a)**. The lifetime in each state was extracted through a double exponential fit to the dwell time histograms with time constants $\tau_{low}^{fast} < \tau_{low}^{slow} < \tau_{high}^{fast} < \tau_{high}^{slow}$ depicted in **Fig. 6(b)**. The two distinct kinetic modes can be seen in the conductance time trace data shown in **Fig. 6(c)**. Association of the time constants with the hybridization (k_{hyb}) and melting (k_{melt}) rates was determined from their dependence on the DNA target concentration. **Fig. 6(d)** shows the Arrhenius plots with 100 nM and 1 μM complimentary target concentration using $k_{hyb} = 1/\tau_{high}^{fast}$ and $k_{melt} = 1/\tau_{low}^{fast}$ for the 1 μM concentration and $k_{hyb} = 1/\tau_{high}^{slow}$ and $k_{melt} = 1/\tau_{low}^{slow}$ for the 100 nM concentration yielding hybridization and melting rates that behave as expected in solution ensemble experiments.

D. Electrostatic Control of DNA Hybridization Kinetics

In a later study, electrostatic control of DNA melting dynamics was demonstrated using the liquid gate to effectively tune the melting temperature (T_m) of a 20-mer oligonucleotide probe and complementary target sequence[6]. Drain-source current time traces with idealized fits are shown in **Fig. 7(a)** for varying temperatures and **Fig. 7(b)** for varying liquid gate bias V_{LG}. From the time traces, we can see that increasing V_{LG} has a similar effect to increasing temperature. **Fig. 8(a)** and **(b)** shows plots of k_{melt} and k_{hyb} for a fully complimentary 20-mer target DNA and a single-base-mismatch- (SNP-) containing target DNA. These plots show electrostatically modulated kinetics very similar to typical thermally modulated kinetics. The correlation between gate-bias-dependent melting at a fixed temperature of 40 ºC to temperature-dependent-melting is depicted in **Fig. 8(c)**. The change in effective melting temperature between the fully complementary target DNA and the SNP-containing target DNA is found to be in good agreement with the expected difference in T_m. A calibration curve between the liquid-gate bias and temperature is shown in **Fig. 8(d)**. This all-electronic approach utilizing the liquid gate voltage as a proxy for temperature in measuring DNA hybridization kinetics is a unique and powerful feature of the smFET device architecture.

E. Aptamer-smFETs for Detection of Small Molecules

Recently, we have investigated the use of single-stranded DNA stem loop structures, also known as aptamers, as probes for the detection of small molecules. Aptamer sequences can be selected to have a high affinity towards a target molecule of interest and low affinity to interferents. Binding to a specific target induces conformational changes of the negatively charged phosphodiester backbone resulting in a local gating effect in the CNT channel. **Fig. 9(a)** shows a drain-source current time trace of a smFET functionalized with an aptamer selected to have a high affinity to serotonin (K_D = 30 nM) in 1 × PBS. While **Fig. 9(b)** shows no noticeable change from the introduction of dopamine (100 nM) into the solution, introduction of serotonin (50 nM) causes two-state fluctuations in the smFET conductance as shown in **Fig. 9(c)**. The serotonin aptamer is known to undergo a conformational change induced by binding to serotonin that extends the negatively charged backbone away from the CNT surface[7]. The positive change in charge at the p-type CNT surface produces a local gating effect, decreasing the conductivity and producing the downward steps in current observed in **Fig. 9(c)**. **Fig. 9(d)** shows the dependence of the downward steps on the concentration of serotonin which saturate near the expected K_D value for the aptamer.

III. CMOS Integration

CMOS integration of smFET devices is necessary to achieve large arrays, a prerequisite for use of these devices in any molecular diagnostic applications. Fabrication can be performed in one of several ways, through dielectrophoresis[8], through spin-cast deposition[4] or through mechanical transfer from the growth substrate[9]. The yield and CNT quality from the first two manufacturing approaches significant impede their usefulness. We have instead relied almost exclusively on mechanical transfer. One of the more successful approaches used a polycarbonate (PPC) transfer process originally developed for graphene device fabrication[10]. It is often necessary to perform additional process to make the CMOS substrate amenable to this transfer, processing that planarizes the substrate while presenting appropriate vias through a dielectric surface for contacting to the CNTs. The density of nanotubes on the growth substrate is optimized to produce the maximum yield, as defined by electrode pairs bridged by a single CNT, on the CMOS substrates.[9]

References

[1] B. R. Goldsmith *et al*., *Nano Lett.,* vol. 8, no. 1, pp. 189-194, Dec. 2007.
[2] J. Jadwiszczak *et al*., *ACS Nano*, vol. 16, no. 1, pp. 1639-1648, Jan. 2022.
[3] H. Wilson *et al*., *J. Phys. Chem. C*, vol. 120, no. 3, pp. 1971-1976, Jan. 2016.
[4] Y. Lee *et al*., *ACS Nano*, vol. 12, no. 10, pp. 9922-9930, Sep. 2018.
[5] S. Sorgenfrei *et al*., *Nat. Nanotechnol*, vol. 6, pp. 126-132, Jan. 2011.
[6] S. Vernick *et al*., *Nat. Commun.*, vol. 8, no. 15450, May 2017.
[7] N. Nakatsuka *et al*., *Science*, vol. 362, no. 6412, pp. 319-324, Sep. 2011.
[8] S. Sorgenfrei *et al*., *Appl. Phys. Lett.*, vol. 94, 053105, Feb. 2009.
[9] S. B. Warren *et al*., *Nano Lett.*, vol. 16, pp. 2674-2679, Mar. 2016.
[10] L. Wang *et al*., *Science*, vol. 342, no. 6158, pp. 614-617, Nov. 2013

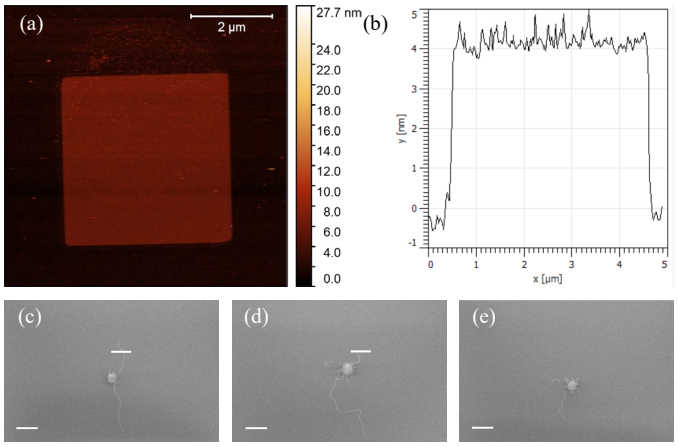

Fig. 1. Atomic force microscope (a) topological scans and (b) a single line scan of a Co catalyst point. (c), (d), (e) Scanning electron micrographs of as-grown CNTs from Co catalyst points. The scale bars are 10 µm.

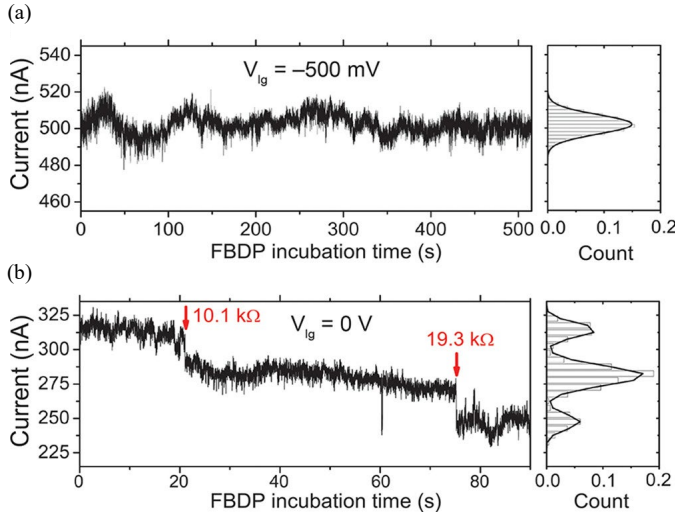

Fig. 3. (a) A representative current time trace for a CNT FET after introduction of 72 µM FBDP solution with V_{LG} = -500 mV and V_{DS} = 50 mV. Current histogram (right) shows a single Gaussian distribution. (b) Representative current time trace for another CNTFET after introduction of 10 µM FBDP solution with V_{LG} = 0 V and V_{DS} = 50 mV. Red arrows indicate times at which discrete downward steps in current are observed. Current histogram shows three Gaussian distributions indicating that the steps are

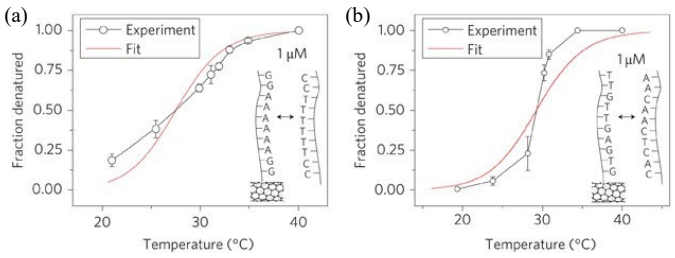

Fig. 5. (a) Melting curves extracted from smFET two-level conductance fluctuations for (a) probe DNA NH_2-5′-GGAAAAAAGG-3′ and (b) probe DNA NH_2-5′-GTGAGTTTGTT-3′ and complementary targets with van't Hoff fits (red).

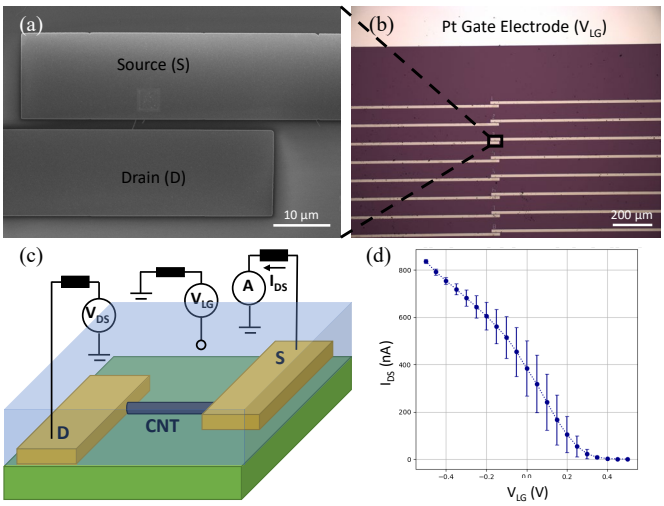

Fig. 2. (a) Scanning electron micrograph of a single CNT FET with Ti (60 nm) source and drain electrodes. (b) Optical microscope image of a CNTFET array and on-chip Pt liquid gate electrode. (c) Schematic illustration of a CNTFET and electrical measurement circuit. (d) CNTFET transfer curve (I_{DS}-V_{LG}) measured in 100 mM phosphate buffer solution with V_{DS} = 90 mV. Each data point is averaged over three bi-directional V_{LG} sweeps each measured at 25 kHz for 1 s. Error bars represent one standard deviation from the average value.

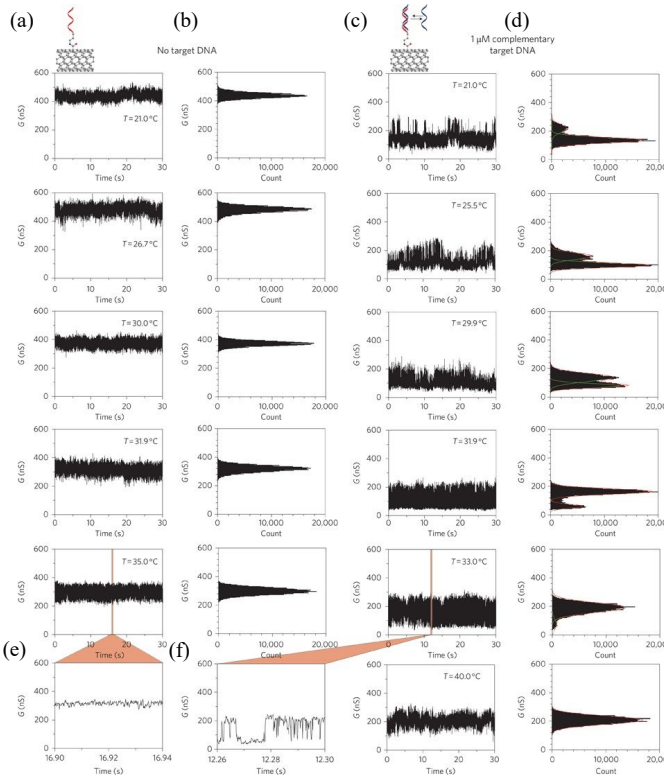

Fig. 4. (a) smFET conductance recordings and (b) histograms for probe DNA NH_2-5′-GGAAAAAAGG-3′ without exposure to complementary DNA target in 1 × PBS with temperature varied from 21 to 35 °C at V_{LG} = 0 V and V_{DS} = 100 mV. (c) smFET conductance recordings and (d) histograms for probe DNA NH_2-5′-GGAAAAAAGG-3′ after exposure to complementary DNA target in 1 × PBS. The two levels are fit to Gaussian distributions. (e),(f) Representative short time intervals before and after exposure to complementary target DNA.

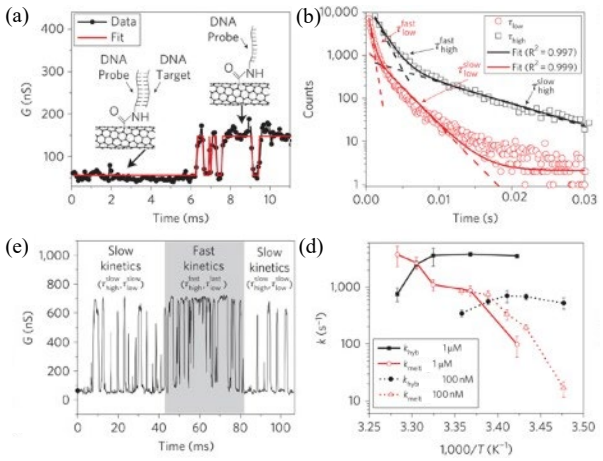

Fig. 6. (a) smFET current time trace (black) and idealized fit (red) from hidden-Markov-model analysis. Inset illustrates associated bound and unbound states of the probe DNA. (b) Example of double exponential fitting at 1 μM complementary DNA target concentration and 32 °C showing fast and slow lifetimes. (c) Representative smFET current time trace showing both fast and slow kinetics. (d) Arrhenius plot showing melting and hybridization rates for 100 nM and 1 M complementary DNA target concentrations. Error bars are calculated from at least sixteen different 15 s intervals.

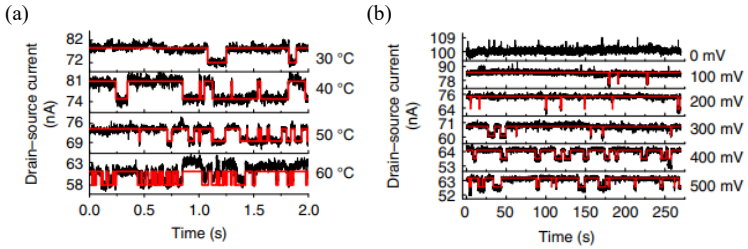

Fig. 7. (a) smFET current time traces (black) and idealized fits (red) for complementary DNA target at a concentration of 100 mM with temperatures ranging from 30 °C to 60 °C. (b) smFET current time traces (black) and idealized fits (red) for complementary DNA target at a concentration of 100 mM measured at a constant temperature of 40 °C with V_{LG} ranging from 0 to 500 mV. When V_{LG} = 0 mV, no melting events are observed. As V_{LG} is increased, the melting rate increases, demonstrating longer and more frequent melting events.

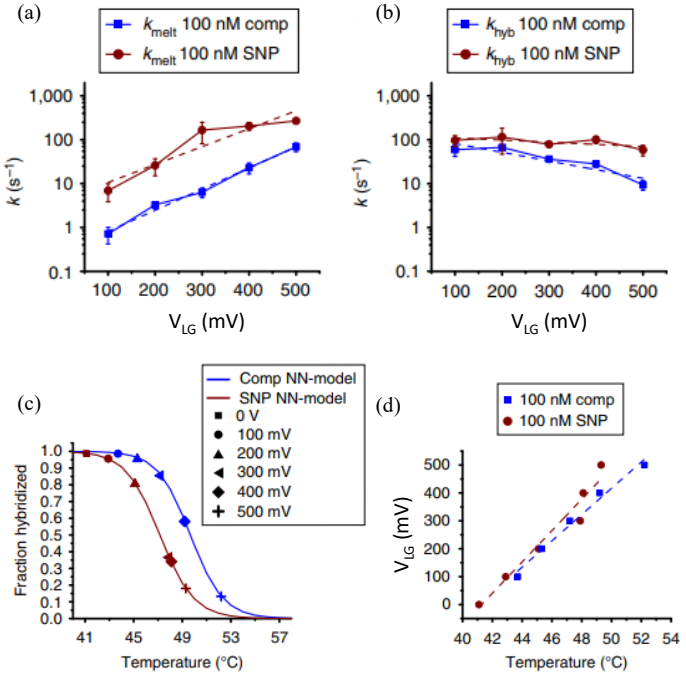

Fig. 8. (a) k_{melt} and (b) k_{hyb} values for the complementary target DNA (blue) and single-base mismatch (SNP) (red). SNP has a smaller activation energy and higher melting rate constant at each V_{LG}. The decrease in k_{hyb} indicates that base-pairing is affected by the repulsive electrostatic force from the gate potential. The SNP does not show this effect since it cannot pair its terminal base. Error bars are calculated from five different 60-s intervals at each temperature. (c) Effective T_m curve showing the hybridized fraction of complementary (blue) and SNP (red) target DNA against their respective nearest-neighbor (NN) models. (d) Calibration curves correlating each liquid gate bias point with an effective temperature.

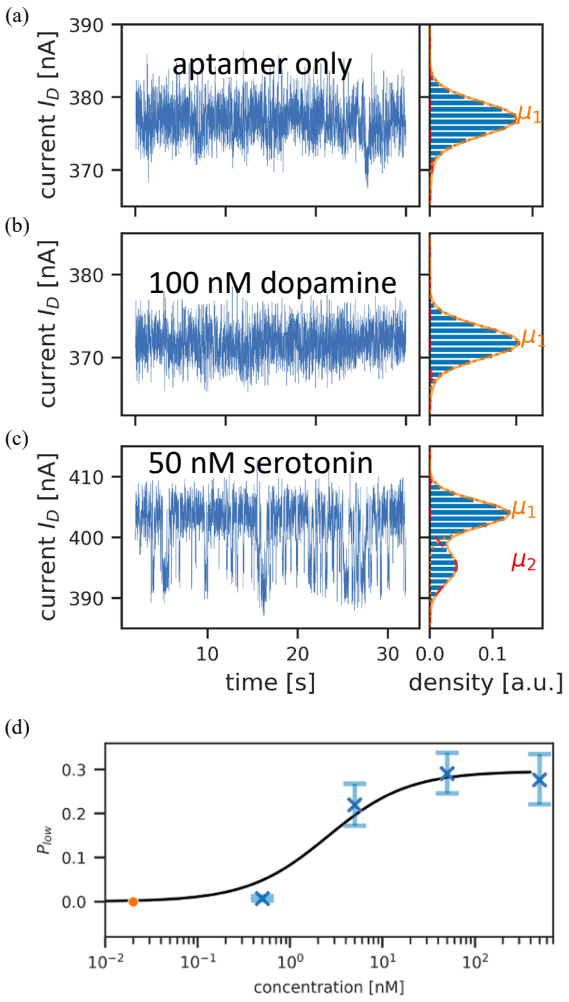

Fig. 9. Current time trace data (left) and corresponding histograms (right) for an smFET functionalized with the serotonin aptamer in (a) 1 × PBS, (b) 100 nM dopamine solution, and (c) 50 nM serotonin solution. Histograms are fit with Gaussian distributions and show a clear transition to discrete two-state behavior when serotonin is introduced. (d) Serotonin concentration dependence of the probability of the smFET current being in the low (P_{LOW}) state. Error bars indicate the confidence interval 0.05-0.95 from bootstrapped fitting (N_{boot} = 2000) of P_{LOW}.